Development of TDR-Sensors for Moist Materials Using HFSS

Norman Wagner, Klaus Kupfer and Eberhard Trinks
Materialforschungs- und -prüfanstalt an der Bauhaus-Universität Weimar
Amalienstr. 13, 99423 Weimar

ABSTRACT: The spatial sensor characteristics of a 6cm TDR flat band cable sensor section was simulated with finite element modelling (High Frequency Structure Simulator-HFSS) under certain real conditions. The complex dielectric permittivity $\tilde{\varepsilon}(\omega,\tau)$ or complex electrical conductivity $\tilde{\sigma}(\omega,\tau) = j\omega\tilde{\varepsilon}(\omega,\tau)$ of saturated and unsaturated soils was examined in the frequency range 50MHz-20GHz at room temperature and atmospheric pressure with a HP8720D- network analyser. The simulation is performed with a λ/3 based adaptive mesh refinement at a solution frequency of 12.5GHz. The electromagnetic field distribution, S-parameter and step responses were examined.

Keywords: lossy dielectrics, finite element modelling, HFSS, dielectric spectroscopy, fractional relaxation

1 Introduction

Soil science, geophysical prospecting, agriculture, hydrology, archeology and geotechnical engineering have benefited greatly from developments in radio and microwave technology. Electromagnetic techniques are used to estimate soil and rock physical characteristics such as water content, density and porosity [28, 23, 18, 19]. Both invasive methods, such as time domain reflectometry [30, 25] and cross borehole radar [6], and noninvasive methods, such as capacity methods and ground penetrating radar [17, 1, 26, 5], are used. Common to all these techniques is the fact that electromagnetic wave interaction depend on dielectric properties of rock or soil deposit through which it travels, which are influenced by chemical composition, mineralogy, structure, porosity, geological age and forming conditions. Besides, several additions have an effect on the dielectric properties like ubiquitous water.
In particular, knowledge of the spatial and temporal variability of water saturation in soils is important to obtain improved estimates of water flow (and its dissolved components) through the vadose zone. Due to its accuracy and potential for automated measurement, TDR has become one of the standard methods to measure spatial and temporal variability of water contents in laboratory soil cores and experimental field plots [10].
In this study the spatial sensor characteristics of a 6cm TDR flat band cable sensor section was simulated with finite element modelling (High Frequency Structure Simulator-HFSS) under certain conditions: (i) in direct contact to surrounding material, (ii) with consideration of a defined gap of variable size filled with air or water and (iii) cable sensor pressed at a borehole-wall.

2 Materials and Methodology

Time domain reflectometry measures the propagation velocity of a step voltage pulse (typical values of a tektronix cable tester: rise time ~200ps, sampling increment Δt ~20ps) with a bandwidth of around 20kHz to ~25GHz (Nyquist-frequency: $f_{Max} = 0.5/\Delta t$). The velocity of this signal is a function of the frequency dependent effective complex permittivity $\tilde{\varepsilon}_{eff}(\omega) = \varepsilon'_{eff}(\omega) - i\varepsilon''_{eff}(\omega)$ of the material through which it travels with potential modification by conductive losses $\varepsilon''_{eff} = \varepsilon''_d + \sigma_{DC}/(\omega\varepsilon_0)$ due to a direct current electrical conductivity σ_{DC} [30]. It is often convenient to consider the analogy of propagation phase velocity $v_P(\omega)$ and attenuation $\beta(\omega)$ of an electromagnetic plane wave:

$$v_P(\omega) = c\sqrt{2}\left(\sqrt{\sqrt{\varepsilon'^2_{eff}(\omega) + \varepsilon''^2_{eff}(\omega)} + \varepsilon'_{eff}(\omega)}\right)^{-1} \tag{2.1}$$

$$\beta(\omega) = \omega\sqrt{\sqrt{\varepsilon'^2_{eff}(\omega) + \varepsilon''^2_{eff}(\omega)} - \varepsilon'_{eff}(\omega)} \cdot \left(c\sqrt{2}\right)^{-1} \tag{2.2}$$

where $\omega = 2\pi f$ is the angular frequency and c the velocity of light [23, 25]. Hence, any modulation of an electromagnetic wave in a real medium will propagate at a group velocity according to the Rayleigh equation [7]

$$v_g = \frac{d\omega}{dk} = v_P\left[1 - \frac{f}{v_P}\frac{dv_P}{df}\right]^{-1}. \tag{2.3}$$

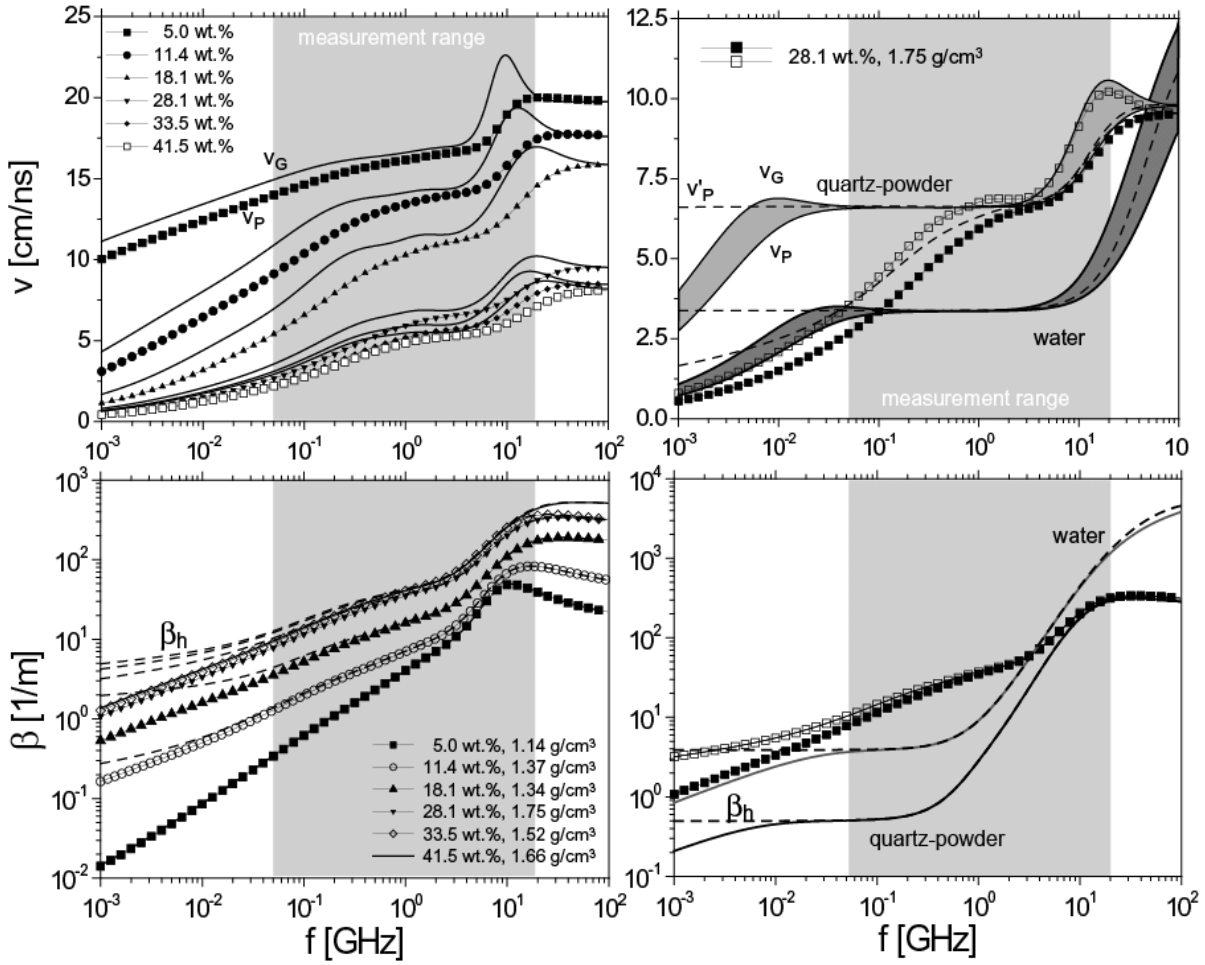

Fig. 1: (top) Phase velocity v_P, high frequency approximation v'_p, corresponding group velocity v_G and (bottom) attenuation β according to (2.2). Also included corresponding high frequency approximation β_h of (left) a sand-bentonite mixture (SB 50/50) with different gravimetric water content c_W and bulk density D (see section 3, Tab. 1, Fig. 2). (right) Comparison of a millisil® quartz powder (median grain size $11\,\mu m$, water content c_W=25.47wt.%, bulk density D=1.55g/cm^3, $\sigma_{DC} = 0.012$S/m), natural water ($\sigma_{DC} = 0.041 S/m$) and sand bentonite mixture SB 50/50-4 (c.f. Tab. 1, section 3).

The flat band cable of length l consists of three strip conductors embedded in a polyethylene band [15, 19]. The effective group or phase velocity of the signal in a perfect dielectric (pure

real $\varepsilon_r = \tilde{\varepsilon} = const.$ without dispersion and conducting losses) surrounding the cable sensor is in principle only a crude approximation especially at frequencies $f < 1GHz$ and $f > 10GHz$ for real soils (c.f. Fig. 1)

$$v_P' = v_g = \frac{2l}{t} = \frac{c}{\sqrt{\varepsilon_r}} \tag{2.4}$$

where t is two way travel time. Considering anomalous dispersion equation (2.4) is referred to as a high frequency approximation of phase velocity (Fig. 1). In contrast the high frequency attenuation approximation for real soils works considerably well (c.f. Fig. 1)

$$\beta_h(\omega) = \frac{\omega\varepsilon_0\varepsilon_{eff}''}{\sqrt{\varepsilon_{eff}'}} Z_0 \tag{2.5}$$

with impedance Z_0 and permittivity ε_0 of free space. We now consider the soil as a four-phase medium composed of: air, quartz grain, water and clay. In the particular case of spatial TDR the surrounding medium in the direction oft the band cable is described by a relative effective permittivity $\tilde{\varepsilon}_{eff}(\omega, \tau, x)$. It depends on position x, angular frequency ω and contribution due to several relaxation processes via relaxation time $\tau(T, p)$ on absolute temperature T and pressure p

$$\tau_i(T, p) = \kappa_i \frac{h}{k_B T} \exp\left(\frac{E_{a,i}(T, p)}{RT}\right). \tag{2.6}$$

Herein, h denotes the Planck-constant, k_B-Boltzmann constant, $\kappa_i \approx 1$ the transmission coeffitient, R gas constant and $E_{a,i}(T, p) = \Delta G_i(T, p) + T\Delta S_i(T, p)$ activation energy of the $i-th$ process [14]. Dielectric loss spectra of saturated and unsaturated soils very often show a marked deviation from simple Debye-behaviour [11, 12, 13, 18]. Based on the theory of fractional time evolutions Hilfer [9] derived a Jonscher type function [16] for the complex frequency dependent dielectric permittivity of amorphous and glassy materials

$$\tilde{\varepsilon}_{eff,i}(\omega, \tau_i) - \varepsilon_\infty = \frac{\Delta\varepsilon_i}{\left(j\omega\tau_i\right)^{\alpha_i} + \left(j\omega\tau_i\right)^{\beta_i}}. \tag{2.7}$$

with high frequency limit of permittivity ε_∞, relaxation strength $\Delta\varepsilon_i$, angular frequency ω and stretching exponents $0 \le \alpha_i, \beta_i$ similar to the familiar empirical Havriliak and Negami [8], Cole-Cole [2], Cole-Davidson [4] or Kohlrausch-Williams-Watts [33] dispersion and absorption functions. For the particular case $\alpha_i = 0$ and $\beta_i = 1$ (2.7) transforms to the Debye model.

3 Experiments

The complex dielectric permittivity $\tilde{\varepsilon}(\omega, \tau)$ of saturated and unsaturated soils was examined in the frequency range 50MHz-20GHz at room temperature and atmospheric pressure with a HP8720D- network analyser. This was performed using a combination of open-ended coaxial-line (HP85070B) and coaxial transmission line technique (sample holder (7x16x100)mm^3). Different natural and synthetic soils were investigated. Here, we present our results for

synthetic soil SB50/50. It is a mixture of 50wt.% sand (grain size <2mm) and 50 wt.% bentonite (Calcigel®: 71wt. % Ca- dioctahedral smectite, 9wt.% illite/dioctahedral mica, 1wt.%kaoline, 1wt.% chlorite, 9wt.% quartz, 5wt.% feldspar, 2wt. % calcite, 2wt.% dolomite) with dry density D_{dry}=1.33g/cm^3. The synthetic soil samples were incrementally wetted from air dry up to saturation with natural water and equilibrated 12h. After each dielectric measurement bulk density D as well as gravimetric water content c_W were determined.

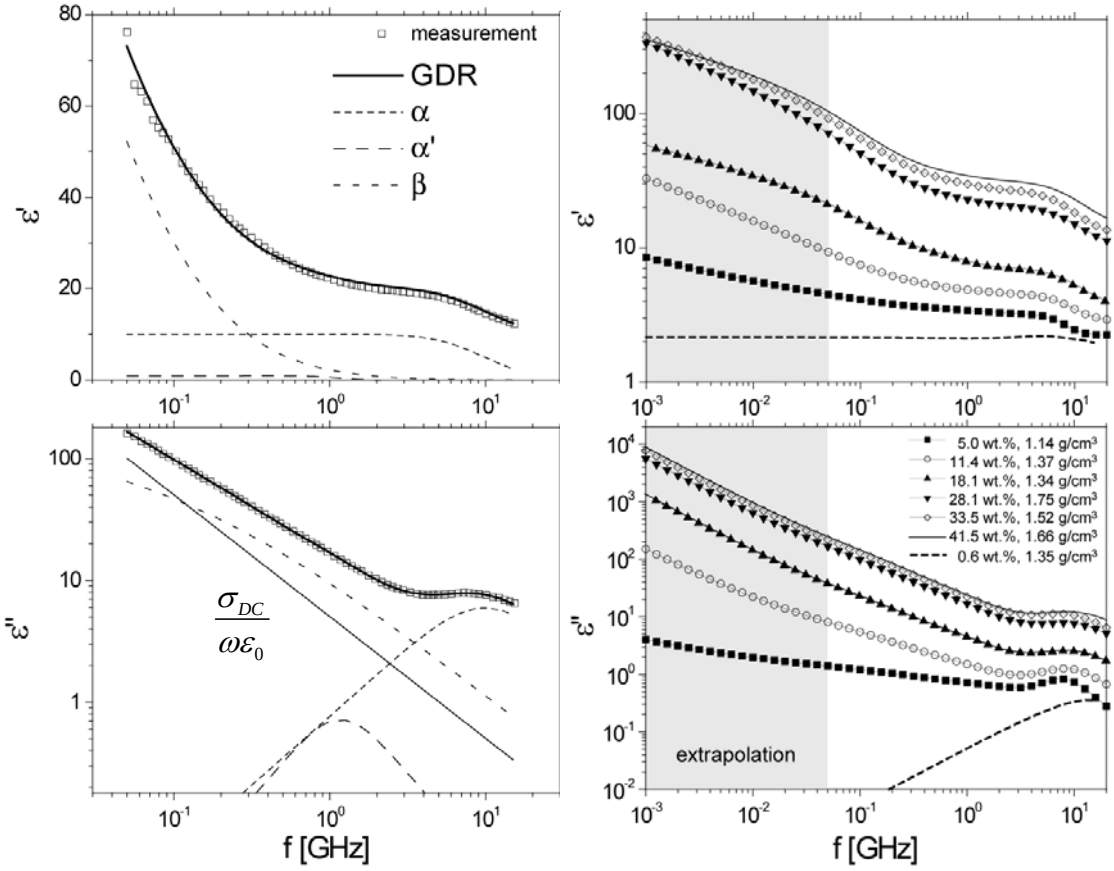

Fig. 2: (left) Complex relative dielectric permittivity $\tilde{\varepsilon} = \varepsilon' - i\varepsilon''$ as a function of frequency with GDR-fit (see text). (right) Dispersion and absorption curve of sand-bentonite-mixture (SB50/50) for different seven water contents c_W and bulk densities D.

Three relaxation processes are assumed to act in the investigated frequency-temperature-pressure range: one primary α-process (main water relaxation) and two secondary (α', β)-processes due to clay-water-ion interactions (bound water relaxation and the Maxwell-Wagner effect). The effective permittivity of a multiphase mixture $\tilde{\varepsilon}_{eff}$ can be determined by the complex relative permittivity of water $\tilde{\varepsilon}_W$, bound water $\tilde{\varepsilon}_{BW}$, the contribution due to clay-water-ion interaction $\tilde{\varepsilon}_{Clay}$ as well as the real and constant permittivity of quartz grain $\varepsilon_{Sand} = 4.5$ and air ε_{air} [28, 23, 27, 29, 13, 14, 3]. The dielectric relaxation behaviour of each process is described by a fractional relaxation model according to (2.7) considering relaxation time distributions $H(\tau)$. This allows the complete spectrum to fit as a function of water content c_W and bulk density D with the use of a generalized dielectric response (GDR):.

$$\tilde{\varepsilon}_{eff}(c_W, D) - \varepsilon_\infty = \sum_{i=1}^{3} \frac{\Delta\varepsilon_i(c_W, D)}{\left(j\omega\tau_i(c_W, D)\right)^{\alpha_i(c_W, D)} + \left(j\omega\tau_i(c_W, D)\right)^{\beta_i(c_W, D)}} - j\frac{\sigma_{DC}(c_W, D)}{\omega\varepsilon_0}. \quad (3.1)$$

A Levenberg-Marquardt algorithm [20] is used to find best GDR fitting parameters (Tab. 1).

Tab. 1: Parameters of the three relaxation processes from GDR-fitting ($i=[\alpha,\alpha',\beta]$); water content c_W and bulk density D of SB-50/50.

	SB50/50-1	**SB50/50-2**	**SB50/50-3**	**SB50/50-4**	**SB50/50-5**	**SB50/50-6**
c_W [wt. %]	5,0	11,4	18,1	28,1	33,5	41,5
D [g/cm^3]	1,14	1,37	1,34	1,75	1,52	1,66
ε_∞	2,3	2,9	3,6	12,6	12,6	13,6
$\Delta\varepsilon_\alpha$	0,7	1,5	3,5	9,9	13,7	17,8
τ_α [ps]	20	18	16	16	18	15
α_α (fixed)	0	0	0	0	0	0
β_α	1,38	1,23	1,1	1,12	1,14	1,07
$\Delta\varepsilon_{\alpha'}$	0,41	0,33	0,7	0,88	1,83	1,63
$\tau_{\alpha'}$ [ps]	73	111	130	136	136	145
$\alpha_{\alpha'}$ (fixed)	0	0	0	0	0	0
$\beta_{\alpha'}$	0,95	1,11	1,2	1,3	1,22	1,27
$\Delta\varepsilon_\beta$	0,96	5,55	16,5	69,04	90,73	103,08
τ_β [ns]	0,53	0,87	1,37	0,93	1,19	1,32
α_β (fixed)	1	1	1	1	1	1
β_β	0,32	0,35	0,21	0,38	0,3	0,26
σ_{DC} [mS/cm]	4E-4	0,074	0,73	2,8	4,21	4,84

4 HFSS Simulation

The transfer or scattering function $S_{i,j}(\omega)$ of the flat band cable section (Fig. 3) was simulated by finite element modelling (High Frequency Structure Simulator-HFSS) under certain conditions: (i) in direct contact to the surrounding material (air, water of various salinities, different synthetic and natural soils (sand-silt-clay mixtures)), (ii) with consideration of a defined gap of various size (total high 2mm, 3mm or 5mm) filled with air or distilled water and (iii) cable sensor pressed at a borehole-wall.

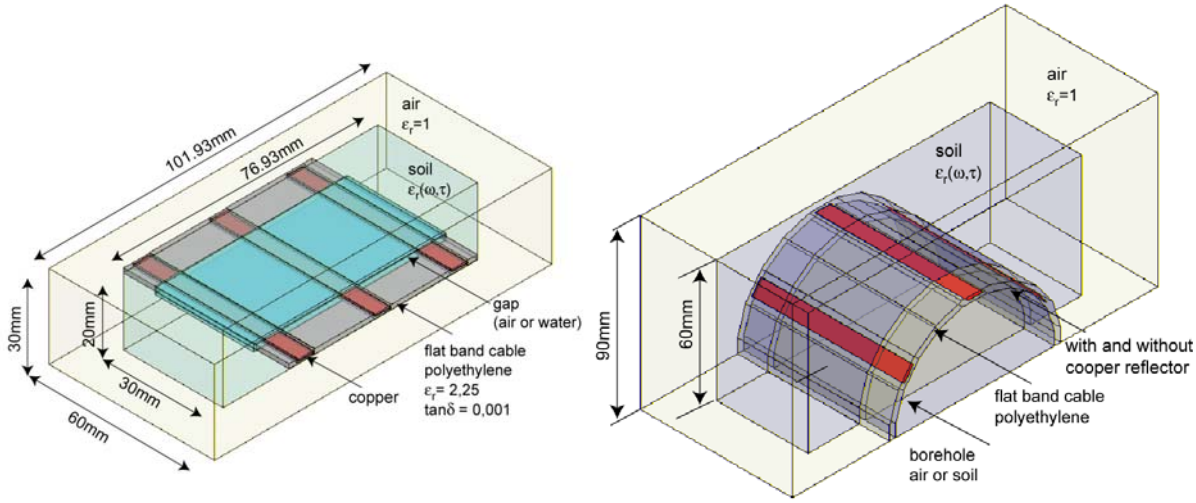

Fig. 3: Model geometry of (left) flat band cable sourounded by saturated and unsaturated soil with a gap filled with air or water and (left) cable sensor pressed at a borehole-wall.

The simulation is performed with a λ/3 based adaptive mesh refinement at a solution frequency of 12.5GHz with an interpolating sweep in frequency range 1MHz-12.5GHz with extrapolation to DC. The electromagnetic field distribution, S-parameter and step response (200ps rise time) of the structure were computed in reflection and transmission mode.

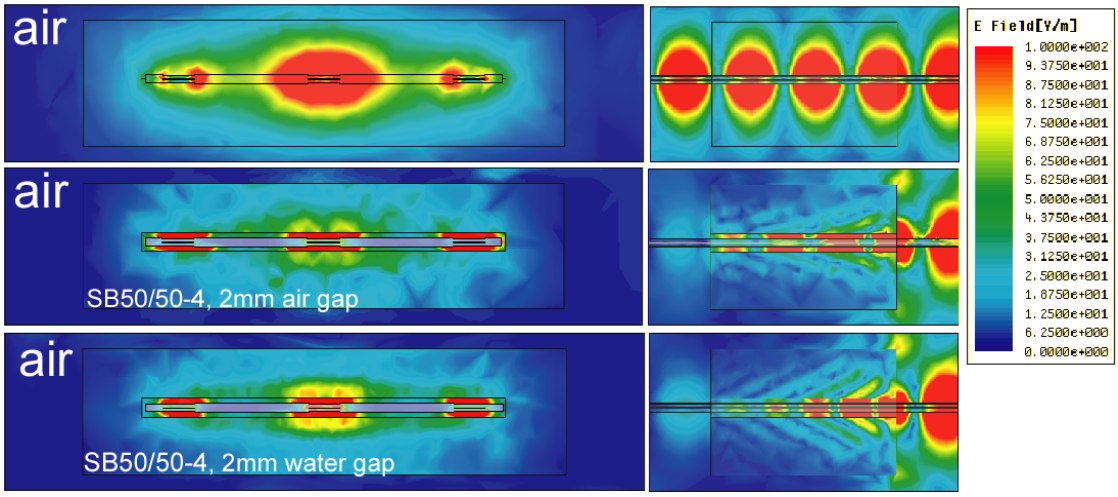

Fig. 4: Electric field distribution @12.5GHz for the investigated flat band cable sourrounded by air, sand-bentonite-mixture (SB_50/50-4) with c_W=28,14wt. % and D=1,79g/cm^3 as well as a defined 3mm air or water gap. (left) Cross section, (right) longitudinal section of middle conductor .

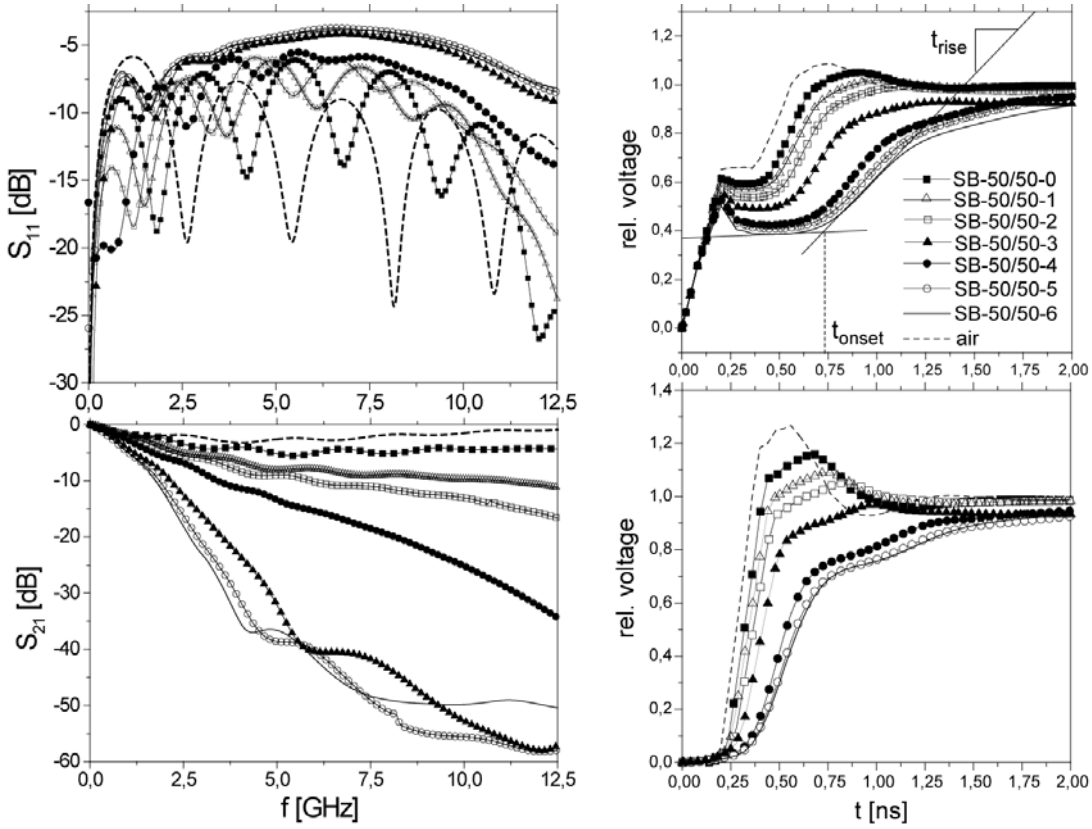

Fig. 5: (left) Input return loss magnitude or reflection coefficitent S_{11} and forward transmission or transmission coeffitient S_{21} as well as (right) TDR-waveform in reflection and transmition mode for simulated flat band cable structure, sourounded by air and sand bentonite mixture of various water contents and bulk densities (see Tab. 1).

5 Discussion and Conclusion

The simulation adequately reproduces the spatial and temporal electrical and magnetic field distribution. High-lossy soils cause in dependence of increasing water content c_W and bulk density D a decrease of TDR signal rise time as well as a strong absorption of multiple reflections (Fig. 5, 6 and Tab. 2). Air or water gap work as quasi wave-guide, i.e. the influence by surrounding medium is strongly reduced (Fig. 4, Tab. 2). Appropriate TDR-travel-time distortions can be quantified (Tab. 2, Fig. 7). Further investigations in combination with reconstruction algorithms have to point out to what extent the accuracy of water content profiles can be determined in high lossy materials.

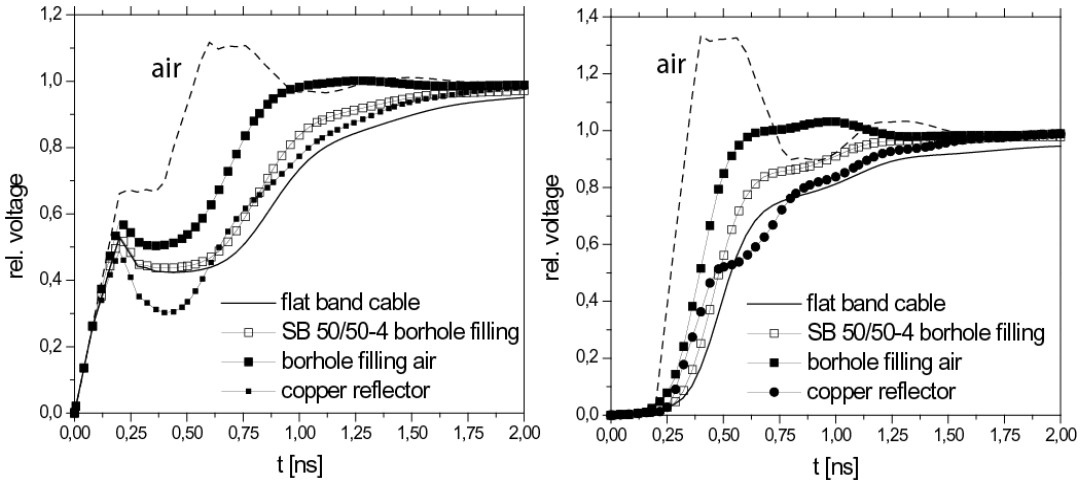

Fig. 6: TDR-waveform in (left) reflection and (right) transmition mode simulated for case (iii) the cable sensor pressed at a borehole-wall with various borehole fillings in compared to the flat band cable sensor.

Tab. 2: Simulation results of different configurations obtained from TDR-data (c.f. Fig.).

Configuration	t_{onset} [ns]	t_{rise} [ns]	ε_{eff} (2.4)	v_{eff} (2.4) [cm/ns]	Z'_{1GHz} [Ω]
flat band cable					
air	0,386	0,533	1,334	25,892	83,8
SB 50/50-0	0,440	0,559	1,727	22,749	84,1
SB 50/50-1	0,466	0,630	1,941	21,461	85,1
SB 50/50-2	0,501	0,663	2,246	19,952	82,0
SB 50/50-3	0,557	0,792	2,769	17,968	81,5
SB 50/50-4	0,678	1,008	4,113	14,742	84,2
SB 50/50-5	0,716	1,137	4,585	13,964	86,0
SB 50/50-6	0,734	1,190	4,820	13,620	81,2
flat band cable, SB 50/50-4, air gap					
5mm	0,445	0,709	1,768	22,484	84,6
3mm	0,491	0,818	2,153	20,377	82,2
2mm	0,554	0,898	2,741	18,059	79,9
flat band cable, SB 50/50-4, distilled water gap					
2mm	0,609	0,899	3,313	16,427	82,2
flat band cable pressed at the borehole wall, SB 50/50-4, different filling					
filling air	0,526	0,722	2,471	19,020	98,0
filling soil	0,631	0,858	3,561	15,846	97,8
reflector	0,493	0,781	2,173	20,282	97,6

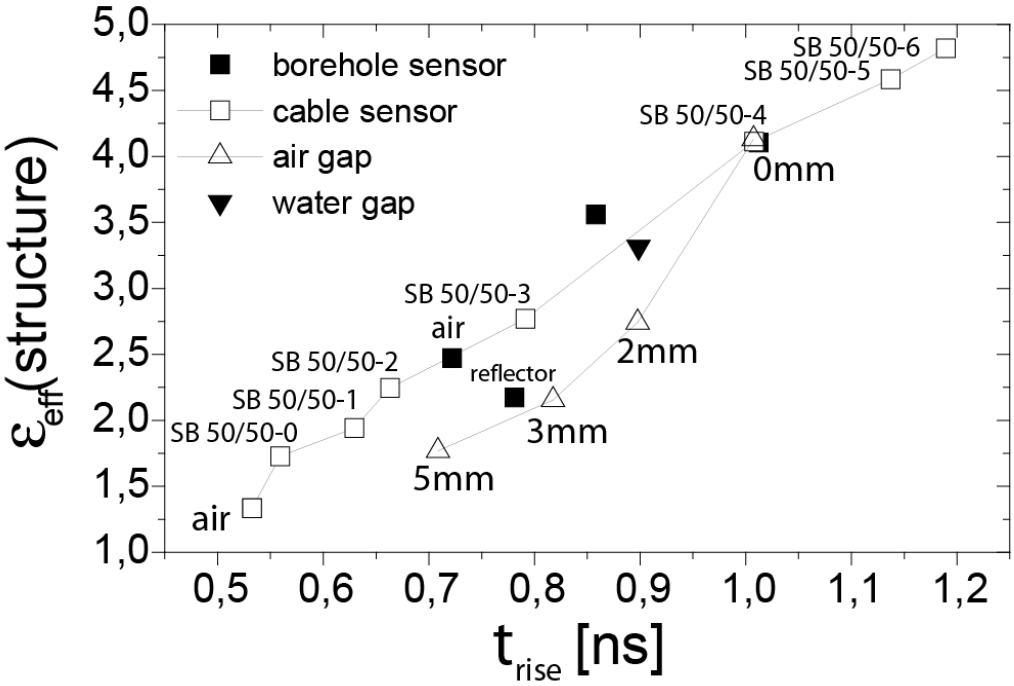

Fig. 7: Real effective relative permittivity ε_{eff} according to equation (2.4) plotted against TDR rise time t_{rise} (in reflection mode) for all sensor configurations and investigated cases.

Acknowledgement

The authors grateful acknowledge the project agency for Water Technology and Waste Management of the BMBF for support of the project 02C0800 and 02WH0487.

References

1. Annan, A. P., Waller, W. M., Strangway, D. W., Rossiter, J. R., Redman, J. D., Watts, R. D. geophysics, 40, 2, (1975), 285-298
2. Cole, K.S., Cole, R.H. Journal of Chemical Physics, 9, (1941), 341-351
3. Cosenza Ph., Tabbagh A. Applied Clay Science, vol. 26, 1-4, (2004), 21-36.
4. Davidson, D., Cole, R. Journal of Chemical Physics, 19, (1951) 1484-1490.
5. Davis, J. L., Annan, A. P. Geophysical Prospecting 37, (1989), 531-551.
6. Fechner,T., Börner,F., Richter,T., Yaramancy,U., Weihnacht,B. Near Surface Geophys. 23,(2004),150-159
7. Forkmann,B., Petzold, H. VEB Deutscher Verlag für Grundstoffindustrie Leipzig 1989
8. Havriliak S., Negami S. Polymer, 8, (4), (1967), 161-210.
9. Hilfer, R. Phys. Rev. E, 65, (2001), 061510
10. Heimovaara, T.J., Huisman, J.A., Vrugt, J.A., Bouten, W. Vadose Zone J. 3, (2004) , 1128-1145
11. Hoekstra, P., Delaney, A. Journal of Geophysical Research, 79, 11, (1974), 1699-1708
12. Hollender, F., Tillard, S. geophysics 63, 6, (1998), 1933-1942
13. Ishida Journal of Colloid and Interface Science 268 (2003) 121-126
14. Ishida, T., Makino, T., Wang, C. Clays and Clay Minerals, 48, 1, (2000), 75-84
15. Hübner, C., Schlaeger, S., Becker, R., Scheuermann, A., Brandelik, A., Schädel, W. and Schuhmann, R.: in K. Kupfer (Ed.), Electromagnetic Aquametry. (2005) Springer
16. Jonscher, A. K. Nature, 267, (1977), 673-679
17. Katsube, T.J., Collet L.S. in Strens, R. G. J.: The Physics and Chemistry of Minerals and Rocks. John Wiley & Sons,London (1974), 279-295
18. Kelleners,T.J., Robinson,D.A., Shouse,P.J., Ayars,J.E., Skaggs, T.H. Soil. Sci. Soc. Am. J. 69,(2005),67-76
19. Kupfer, K. Trinks, E. in K. Kupfer (Ed.), Electromagnetic Aquametry, (2005) Springer-Verlag
20. Marquardt, D. SIAM J. Applied Math 11, (1963), 431-441
21. Martinez, A. and Byrnes, A. P. Current Research in Earth Sciences, Bulletin 247, 1 (2001) 2-13
22. Nyquist, H. Trans. AIEE, 47, (1928) 617-644.

23. Olhoeft, G. R. in Y. S. Touloukian (eds). Physical Properties of Rocks. Hemisphere (1981) 257-329.
24. Parnadi, Ir. W. W. PhD-Thesis, TU Bergakademie Freiberg, 2001
25. Robinson, D. A., Jones, S. B., Wraith, J. M., Or, D., Friedman, S. P. Vadose Zone J 2 (2003) 444-475
26. Rossiter, J.R., Annan, A. P., Strangway, D. W., Redman, J. D., Watts, R. D. 40, 2, (1975), 299-308
27. Saarenketo, T. Journal of Applied Geophysics, 40, (1998), 73–88
28. Shen, L.C., Savre, W.C., Price, J.M., Athavale, K. geophysics, 50, 4, (1985), 692-704
29. Sihvola, A. Iee Electromagnetic Waves Series, 47 (2000), INSPEC, Inc.
30. Topp, G. C., Davis, J.L., Annan, A.P. Water Resour. Res. 16(1), (1980), 574-588
31. Wang, J. R., Radio Science, 15, (1980), 977-985.
32. Wang, J. R., Schmugge, T. J. IEEE Trans. Geosciences and Remote Sensing, GE-18, (1980), 288-295.
33. Williams, G., Watts, D.C. Trans. of the Faraday Society, 66, (1970), 80-85

Corresponding author: Norman Wagner, Materialforschungs- und –prüfanstalt an der Bauhaus-Universität Weimar, Amalienstr. 13, 99423 Weimar, Phone: +49-3643-564221, Fax: +49-3643-564204,
e-mail: norman.wagner@mfpa.de